SAND--95-8604C
Conf-950731--3

DIRECT NUMERICAL SIMULATION OF TURBULENT NON-PREMIXED METHANE-AIR FLAMES

Jacqueline H. Chen and John M. Card
Sandia National Laboratories
Combustion Research Facility
Livermore, California 94550-0969 USA

Mark Day
Department of Mechanical Engineering
Stanford University
Stanford, California 94305 USA

Shankar Mahalingam
Department of Mechanical Engineering
University of Colorado at Boulder
Boulder, Colorado 80309-0427 USA

ABSTRACT

Turbulent non–premixed stoichiometric methane–air flames have been studied using the direct numerical simulation approach. A global one–step mechanism is used to describe the chemical kinetics, and molecular transport is modeled with constant Lewis numbers for individual species. The effect of turbulence on the internal flame structure and extinction characteristics of methane–air flames is evaluated. The flame is wrinkled and in some regions extinguished by the turbulence, while the turbulence is weakened in the vicinity of the flame due to a combination of dilatation and a 25:1 increase in kinematic viscosity across the flame. Reignition followed by partially–premixed burning is observed in the present results. Local curvature effects are found to be important in determining the local stoichiometry of the flame, and hence, the location of the peak reaction rate relative to the stoichiometric surface. The results presented in this study demonstrate the feasibility of incorporating global–step kinetics for the oxidation of methane into direct numerical simulations of homogeneous turbulence to study the flame structure.

INTRODUCTION

The present study is part of a larger effort to evaluate the effect of different levels of reduction of fuel oxidation kinetics on methane–air turbulent non–premixed flame structure and extinction characteristics. In the present paper, the results from direct numerical simulation (DNS) with a single–step mechanism for methane–air combustion using empirically derived rate constants are presented. The transport model in the present DNS accounts for individual Lewis numbers for each of the species and differences in molecular weight between species. Previous DNS studies [1, 2, 3] have assumed equal

molecular weights for all of the species and have assumed a stoichiometric mixture fraction of 0.5. In the present DNS, the stoichiometric surface corresponds to a mixture fraction of 0.055.

To quantify the flame structure and the dynamics of extinction, the interaction between a non–premixed laminar flame and isotropic decaying turbulence is studied. The flame structure is determined in terms of curvature, strain–rate and scalar dissipation rate.

GOVERNING EQUATIONS AND NUMERICAL METHOD

The governing equations are the continuity, momentum, species, and energy equations written in Cartesian tensor notation as follows:

$$\frac{\partial \rho}{\partial t} + \frac{\partial \rho u_j}{\partial x_j} = 0 \,, \tag{1}$$

$$\frac{\partial \rho u_i}{\partial t} + \frac{\partial \rho u_i u_j}{\partial x_j} = -\frac{\partial p}{\partial x_i} + \frac{\partial \tau_{ij}}{\partial x_j} \,, \tag{2}$$

$$\frac{\partial \rho Y_\alpha}{\partial t} + \frac{\partial \rho Y_\alpha u_j}{\partial x_j} = -\frac{\partial}{\partial x_j}\left(\rho Y_\alpha V_{\alpha j}\right) + \dot{\omega}_\alpha \tag{3}$$

$$\frac{\partial \rho e_t}{\partial t} + \frac{\partial (\rho e_t + p) u_j}{\partial x_j} = \frac{\partial (u_i \tau_{ij})}{\partial x_j} - \frac{\partial q_j}{\partial x_j} \tag{4}$$

where

$$\tau_{ij} = \mu\Big(\frac{\partial u_i}{\partial x_j} + \frac{\partial u_j}{\partial x_i} - \frac{2}{3}\delta_{ij}\frac{\partial u_k}{\partial x_k}\Big) \,, \tag{5}$$

is the stress tensor,

$$e_t = e + \frac{1}{2}\sum_{k=1}^{3} u_k^2, \quad e = \sum_{\alpha=1}^{N} Y_\alpha h_\alpha - \frac{p}{\rho} \tag{6}$$

is the total energy per unit mass of the mixture, e is the internal energy per unit mass, h_α is the enthalpy of species α given by,

$$h_\alpha = h_\alpha^0 + \int_{T^0}^{T} C_{p\alpha}(T')dT', \quad \alpha = 1, \cdots, N \tag{7}$$

where h_α^0 and $C_{p\alpha}$ are the corresponding enthalpy of formation and specific heat at constant pressure respectively. The heat flux vector is given by

$$q_j = -\lambda\frac{\partial T}{\partial x_j} + \rho\sum_{\alpha=1}^{N} h_\alpha Y_\alpha V_{\alpha j} \tag{8}$$

and the species diffusion velocity is

$$V_{\alpha j} = -D_{\alpha N}\frac{1}{Y_\alpha}\frac{\partial Y_\alpha}{\partial x_j}, \quad \alpha = 1, \cdots N-1 \tag{9}$$

where $D_{\alpha N}$ is the binary diffusion coefficient between species α and the N-th species taken to be nitrogen. To ensure that the net diffusion velocity is zero, the constraint $\sum_{\alpha=1}^{N} Y_\alpha V_{\alpha j} = 0$ is enforced to obtain V_{Nj}. The equation of state is

$$p = \rho RT \tag{10}$$

where R is the mixture gas constant given by

$$R = R^0/\bar{W}, \quad \bar{W} = \left[\sum_{\alpha=1}^{N}\left(\frac{Y_\alpha}{W_\alpha}\right)\right]^{-1} \tag{11}$$

where R^0 is the universal gas constant, $\bar{W}$ is the average molecular weight of the mixture, and W_α is the species molecular weight. The mixture averaged thermal conductivity is modeled through the approximation suggested by Smooke [4],

$$\lambda = \bar{C}_p A\left(\frac{T}{T_0}\right)^r \quad \bar{C}_p(T) = \sum_{\alpha=1}^{N} Y_\alpha C_{p\alpha}(T) \tag{12}$$

where $A = 2.58 \times 10^{-4}$ g/cm-sec, $r = 0.7$, and $\bar{C}_p$ is the specific heat of the gaseous mixture. The individual species specific heats are obtained as polynomial functions of temperature using the Chemkin thermodynamic database [5]. The diffusion coefficients are obtained by prescription of Lewis numbers for individual species through

$$D_{\alpha N} = \frac{\lambda}{\bar{C}_p \rho Le_\alpha}. \tag{13}$$

The Lewis number data is obtained from Smooke [4]. For the one-step mechanism, the Lewis numbers for CH_4, O_2, CO_2, and H_2O are 0.97, 1.11, 1.39, and 0.83, respectively. The other symbols in these equations have the usual meaning. Conservation equations for four reacting species are considered (CH_4, O_2, CO_2, and H_2O) and the mass fraction of N_2 is obtained through the relationship $\sum_{\alpha=1}^{N} Y_\alpha = 1$, where $N = 5$.

The dimensionless form of the governing equations is obtained through definition of appropriate reference quantities based on the air stream properties. The sound speed at infinity a_∞, corresponding density ρ_∞, and the dynamic pressure $\rho_\infty a_\infty^2$ are used for the velocity, density, and pressure reference quantities. The reference temperature is $(\gamma_\infty - 1)T_\infty$ where γ_∞ is the ratio of specific heats at temperature T_∞ of the air stream. The reference fluid properties used are μ_∞, λ_∞, and $C_{p\infty}$ corresponding to air at temperature T_∞. A reference length scale L_{ref} is chosen to be the distance between

the fuel and oxidizer jets in the opposed diffusion flame used to initialize all the dependent variables in the computational domain.

The equations are solved using a standard sixth–order accurate compact finite difference scheme (Lele [6]) for approximating spatial derivatives, and a third–order Runge–Kutta scheme for time advancement. A modified version of the Navier–Stokes Characteristic Boundary Condition (NSCBC) procedure originally developed by Poinsot and Lele [7], and suitably modified to account for variable specific heats is implemented. The boundary conditions are periodic in the y direction and non–reflecting in the x direction [1].

The turbulence field is prescribed by an initial two–dimensional turbulent kinetic energy spectrum function

$$E(k) = C_0 \frac{u_0^2}{k_0} \left(\frac{k}{k_0}\right)^4 \exp\left[-2\left(\frac{k}{k_0}\right)^2\right], \tag{14}$$

where k is the wavenumber, k_0 is the wavenumber corresponding to the most energetic eddies, and u_0 is the rms velocity.

INITIAL CONDITIONS AND FLAME PARAMETERS

The reacting flow field in a one-dimensional steady laminar opposed jet diffusion flame configuration including a full 40 step chemical kinetic mechanism was obtained using the Sandia code OPPDIF. Pure methane and air at 1 atmosphere, 300°K with a strain rate of approximately 20 sec^{-1} are the conditions imposed at the fuel and oxidizer jets which are separated by a distance of 1 cm. These correspond to low strain rate conditions. The strained laminar flame solution from OPPDIF was then allowed to relax to an unstrained condition in the DNS code where the one–step kinetic mechanism and the corresponding global rate is the basis for the present study. The rate for the global step: $CH_4 + 2O_2 \rightarrow CO_2 + 2H_2O$ used in the DNS is taken from Bui–Pham [8], namely, $k = 5.2 \times 10^{13} \exp(-14906/T)$ (units are moles, cm, s , K, and KJ/mole). The unstrained one-dimensional laminar flame profile was used to initialize the species mass fraction, temperature, and density fields in the turbulence simulations.

The DNS was initialized in a two–dimensional computational domain with a plane laminar diffusion flame in the center separating fuel on the left half of the domain and oxidizer on the right half of the domain. The velocity field was initialized with the turbulent kinetic energy spectrum given in Eq. (14) over the entire domain with the exception of the region near the outflow boundaries. The turbulent Reynolds number was taken to be 57 based on the Taylor microscale; note that the flame is thicker than the microscale but thinner than the turbulent integral scale.

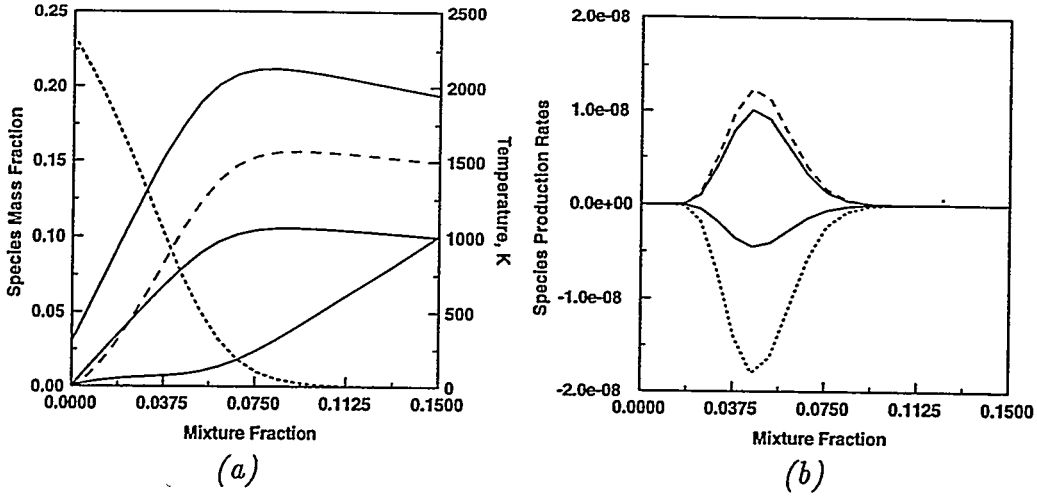

Figure 1. Plane unstrained laminar stoichiometric methane-air nonpremixed flame structure, a) temperature and species mass fraction, and b) species production rates. ——— CH_4, ····· O_2, ---- CO_2, —— H_2O.

RESULTS AND DISCUSSION

Laminar Flamelet Results

Shown in Fig. 1 is the flamelet structure in mixture fraction coordinates for the global one–step reaction mechanism. The mixture fraction is defined in terms of the corresponding element mass fractions given in Smooke [6]. Note in Fig. 1a that the maximum flame temperature of 2250 K is located at the stoichiometric mixture fraction $Z_{st} = 0.055$ and that the temperature gradient, $\frac{\partial T}{\partial Z}$, is larger on the oxidizer side of the flame. The greater extent of the high temperature region in mixture fraction coordinates on the fuel side has implications for the relative strength of the turbulence on the fuel and oxidizer sides of the diffusion flame as will be discussed in the following section.

A distinctive qualitative difference between the one–step and multi–step mechanisms is the width of the reaction zone. In Fig. 1b, it can be seen that the consumption of the fuel extends over a wide range of mixture fraction for the one–step mechanism. The thinness of the fuel–consumption layer in multi–step mechanisms [9] is one of the primary causes of resolution difficulties in direct simulations of turbulent flames. Furthermore, in the one–step approximation, both fuel and oxidizer leak through the reaction zone (Fig. 1a). For multi–step mechanisms, only oxygen leaks through the reaction layer in agreement with numerical calculations employing full detailed mechanisms [9].

Turbulent Flame Structure

The turbulent two–dimensional DNS was postprocessed at 1.0 and 1.5 turbulent eddy turnover times. This is sufficient time for the initial adjustment to occur between the imposed turbulence spectrum and the laminar flame.

For the purpose of evaluating strain rate and curvature effects, the flame surface is located by the stoichiometric mixture fraction, $Z = 0.055$. The flame normal is defined using the local gradient of Z:

$$\mathbf{n} = \frac{-\nabla Z}{\mid \nabla Z \mid} . \qquad (15)$$

The strain rate tangent to the flame surface is given by:

$$S_T = \nabla_T \cdot \mathbf{u} . \qquad (16)$$

Instantaneous isocontours of the vorticity magnitude, temperature, and CH_4 production rate at $t = 1.0$ eddy turnover time are shown in Fig. 2. In these figures the flame is denoted by the stoichiometric mixture fraction $Z = 0.055$.It is evident from Fig. 2a that the vorticity is significantly weakened in the vicinity of the reaction zone. The reduction in vorticity is more pronounced on the fuel rich side of the flame since the temperature remains high for a greater distance away from the flame due to the smaller temperature gradient that exists on this side. The reduction in vorticity in the vicinity of the flame is attributed to a combination of dilatational effects and a substantial increase in the kinematic viscosity with temperature. The ratio of the kinematic viscosity in the reaction zone to that in the fuel freestream is 25:1. As a result of this large rise in kinematic viscosity the turbulence that was initially inside the reaction zone has little effect on stretching or wrinkling the flame. The turbulence is able to penetrate the flame only in regions where the flame is locally extinguished as shown by a comparison of the vorticity magnitude (Fig. 2a) and the reaction rate (Fig. 2c).

Whereas the effect of heat release is to weaken the turbulence, the effect of turbulence is to wrinkle the flame. There are regions where the flame is locally extinguished, clearly shown by the discontinuities in the reaction rate contour lines in Fig. 2c. The extinction is a result of high tangential strain rate experienced by the flame. The correlation of tangential strain rate with reaction rate is shown in Fig. 3, and with the exception of a few points undergoing various stages of extinction, there is a strong positive correlation between tangential strain rate and reaction rate.

At a later time, $t = 1.5$ eddy turnover times, conditions are such that locally the strain rate is reduced in regions with hot products due to heat release. The hot products act as an ignition source, and in locations where both fuel and oxidizer are present, the flame starts to burn again. A comparison of Fig. 4 and Fig. 2c shows a region where reignition occurred. In this region the flame is burning in a partially–premixed mode. The peak reaction rate is 25 percent larger in the partially–premixed region than it is in the main body of the turbulent diffusion flame and, in mixture fraction coordinates shown in Fig. 5, the premixed region exhibits a peak in the reaction rate near $Z = 0.1$ whereas the main body of the turbulent diffusion flame exhibits its peak near the stoichiometric value. Furthermore, the reaction

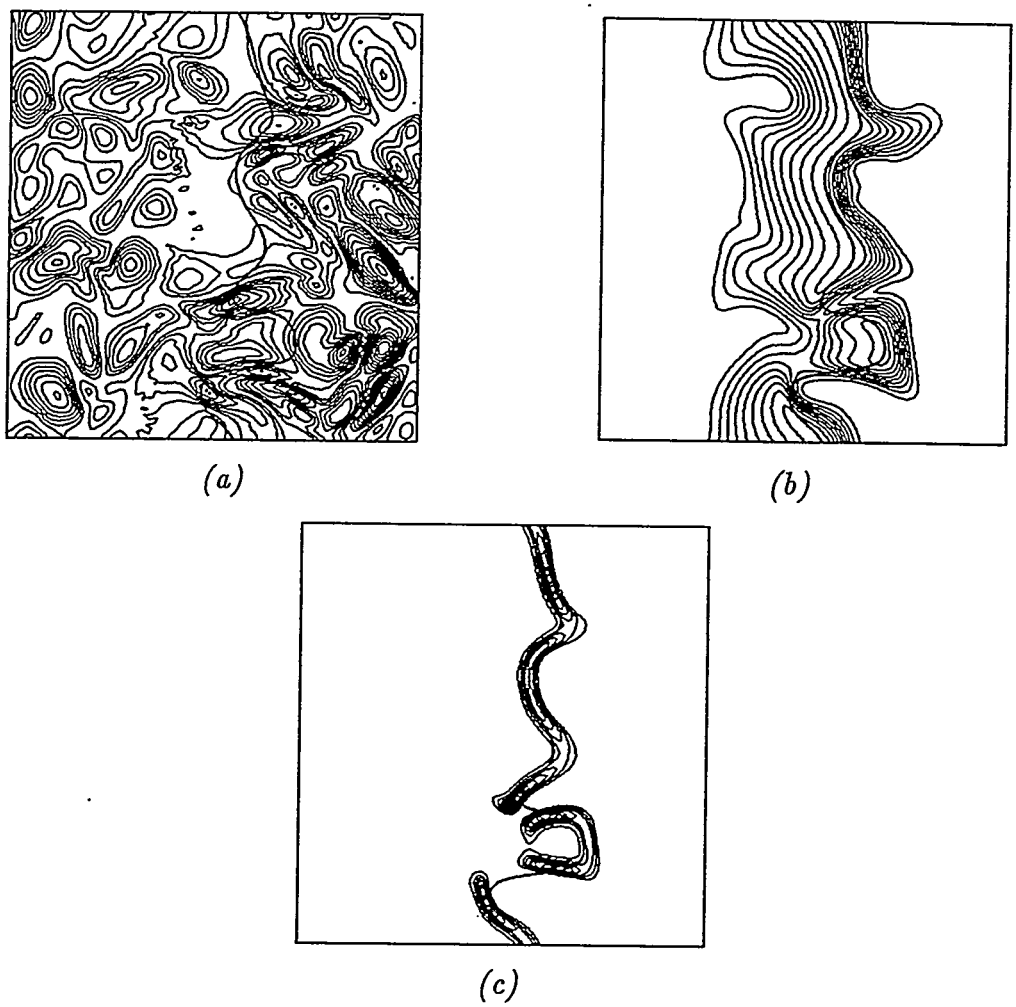

Figure 2. Instantaneous isocontours of turbulent non-premixed methane-air flame at $t = 1.0$ eddy turnover time, a) vorticity magnitude, b) temperature, and c) CH_4 production rate. The solid line denotes the stoichiometric mixture fraction, $Z = 0.055$. The fuel stream is on the left half of the domain and the oxidizer stream is on the right half.

zone for the partially–premixed region is five times broader than the reaction zone for the diffusion flame as is denoted by the two-tiered structure of the CH_4 production rate.

It is also observed from a comparison of the reaction rate contour lines and the stoichiometric mixture fraction line (Fig. 2c) that the flame does not always burn at the stoichiometric mixture fraction. In regions that are curved toward the oxidizer stream the flame has a tendency to burn fuel lean, whereas in regions that are curved toward the fuel stream the flame has a tendency to burn fuel rich. For the global one-step mechanism considered here where the Lewis number of both reactants is near unity, this phenomenon is attributed primarily to a kinematic effect and is particularly pronounced in regions having the greatest curvature. The curvature of the flame surface is given by

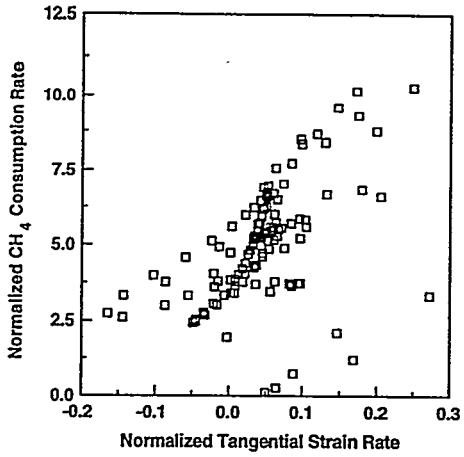

Figure 3. Scatter plot of maximum reaction rate along flame normal versus tangential strain rate.

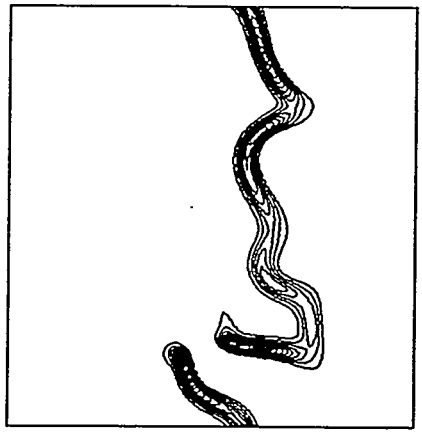

Figure 4. CH_4 production rate at $t = 1.5$ eddy turnover time showing reignition and partially-premixed burning.

$$K = \nabla \cdot \mathbf{n} \ , \tag{17}$$

where positive curvature is defined such that the flame is concave towards the oxidizer stream. As is shown in Fig. 6, in regions that exhibit negative curvature, the defocusing of methane combined with the focusing of oxygen at the flame overcomes the slightly greater mass diffusivity of methane ($Le = 0.97$) over oxygen ($Le = 1.11$). Hence, locally the flame tends to burn lean. In regions that exhibit positive curvature the focusing of methane and defocusing of oxygen combined with the larger mass diffusivity of methane over oxygen leads to a situation where there is an abundance of methane at the reaction zone. Hence, in this situation the flame tends to burn fuel–rich. Lewis number effects may become more significant when fast diffusing radical species are accounted for in multi-step mechanisms for methane–air flames.

To ascertain the influence of local stoichiometry and curvature on

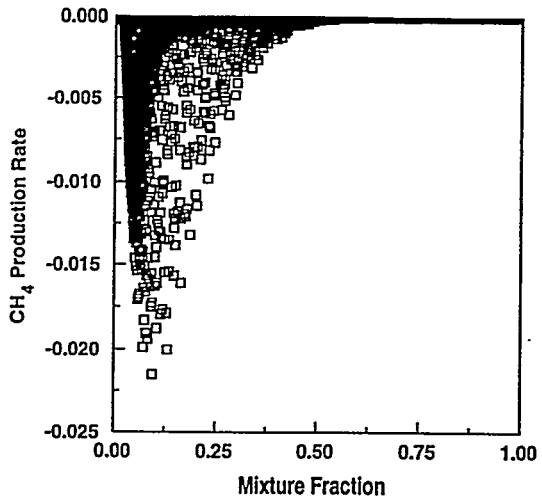

Figure 5. Scatter plot of CH_4 production rate versus mixture fraction at $t = 1.0$ eddy turnover time.

reaction rate we next examine the correlation of the curvature with scalar dissipation rate and reaction rate shown in Figs. 7a and 7b. Note, that in both Figs. 7a and 7b there is a strong positive correlation between curvature and reaction rate and scalar dissipation rate. Large positive values of curvature are associated with maximum values of the reaction and scalar dissipation rates, whereas, large negative values of curvature are associated with minimum values of reaction and scalar dissipation rates. An explanation for this positive correlation is obtained by examining the structure of the scalar dissipation rate (Fig. 8) , a quantity that is representative of the intensity of the small scale mixing. From this figure it is evident that locally fuel-rich stoichiometry ($Z > 0.055$) results in more intense small scale mixing than fuel–lean stoichiometry. Note, that the peak dissipation rate occurs at a mixture fraction of one–half. Therefore, regions of the flame that are concave towards the oxidizer side (positive curvature), tend to experience more intense small scale mixing, and therefore exhibit higher reaction rates and are more likely to become extinguished due to strain rate than regions in the flame that are concave towards the fuel stream (negative curvature). The curvature and Lewis number effects discussed here suggest that the peak reaction and scalar dissipation rates may not be coincident with the stoichiometric surface.

Due to the weakening of the turbulence inside and near the flame as a result of the heat release, the primary wrinkling of the flame is attributed to the turbulence outside of the reaction zone. Therefore, the turbulent flame can be modeled as an ensemble of strained laminar flames for the present DNS. In regions of large positive curvature a fuel–rich strained laminar flame could be used to model the turbulent flame structure, whereas a fuel–lean strained laminar flame could appropriately model regions of large negative curvature. Using high activation energy asymptotic analysis applied to a stagnant one–dimensional laminar diffusion flame with unity Lewis numbers,

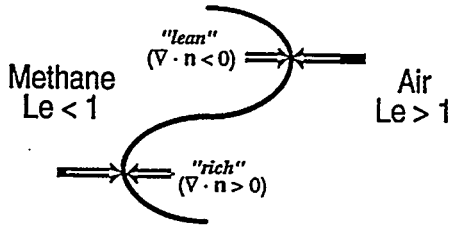

Figure 6. Schematic showing the effect of Lewis number and curvature on the local stoichiometry. Length of thin arrows denotes relative mass diffusivity of methane and air due to unequal Lewis numbers. Length of thick arrows denotes the relative mass diffusion of methane and air due to the net effect of Lewis number and curvature.

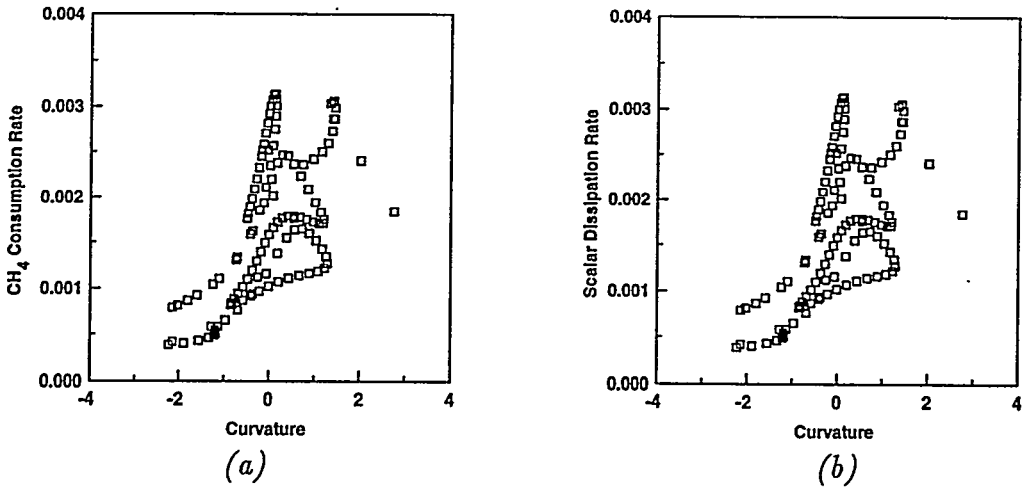

Figure 7. Scatter plot of mean curvature and a) CH_4 production rate, and b) mixture fraction scalar dissipation rate.

Wichman [11] showed that by varying the equivalence ratio such that the flame was either oxygen rich or fuel rich, a separation in mixture fraction coordinates between the stoichiometric surface and the peak reaction rate and peak temperature was achieved. Consistent with what is observed in the present turbulent DNS, he found that the peak reaction rate occurred on the fuel side for fuel–rich conditions and on the oxidizer side for fuel–lean conditions. However, in the present DNS study, curvature effects are primarily responsible for the separation between the peak reaction rate and stoichiometric surface.

Scatter plots of the temperature and species concentrations in mixture fraction coordinates are shown in Fig. 9. The maximum temperature (Fig. 9a) occurs near the stoichiometric mixture fraction, $Z = 0.055$. Consistent with the physical representation of the flame, the presence of both high and low values of the temperature suggests that there are regions in

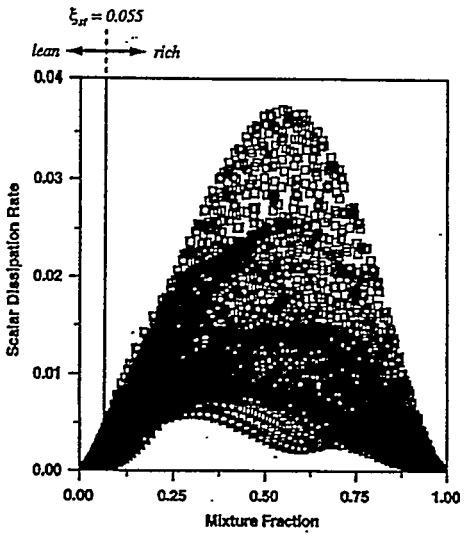

Figure 8. Scatter plot of mixture fraction scalar dissipation rate and mixture fraction at $t = 1.0$ eddy turnover time.

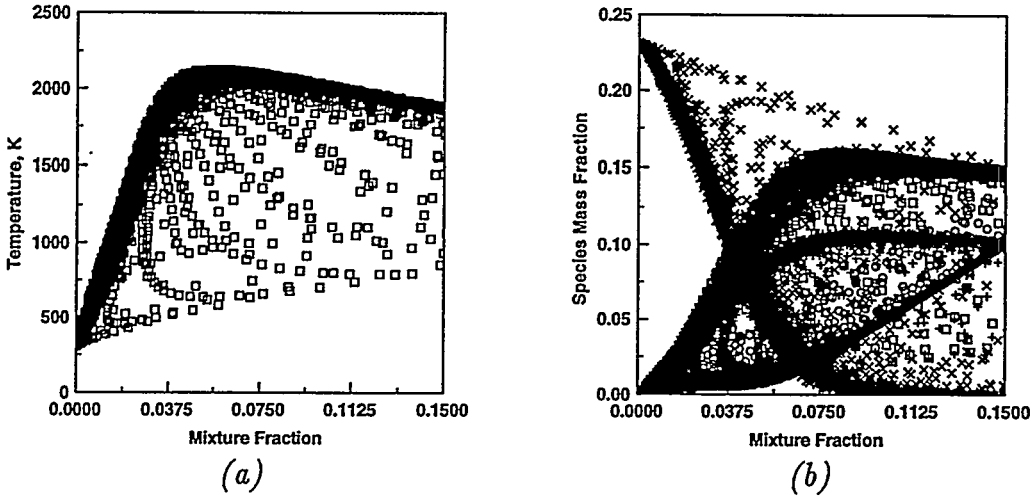

Figure 9. Scatter plot in mixture fraction coordinates at $t = 1.0$ eddy turnover time of a) temperature, and b) species mass fraction (o CH_4, × O_2, □ CO_2, + H_2O).

the flame that are near equilibrium as well as other regions that are undergoing various stages of extinction as indicated by the spread of points between the equilibrium and pure mixing limits. The species concentrations in Fig. 9b also provide evidence of regions undergoing various stages of extinction. Furthermore, it is evident that there is leakage of both CH_4 and O_2 in this one–step model.

CONCLUDING REMARKS

Results from the DNS demonstrate that two-dimensional simulations of turbulent non–premixed methane–air flames incorporating a single-step mechanism are feasible. Extensions to multi–step mechanisms require resolving the fuel consumption layer of the flame, a region that is approximately an

order of magnitude smaller than the overall flame thickness. The following is a summary of the key results obtained from the single–step turbulent non–premixed DNS:

- The reaction rate and scalar dissipation rate are strongly correlated with the local curvature of the flame.
- The local stoichiometry of the flame is correlated with the curvature and results in a separation between the stoichiometric surface and the peak reaction rate.
- Burning "fuel–rich" results in a higher scalar dissipation rate, and hence, a higher reaction rate; local extinction is more likely to occur in fuel rich zones.
- Extinction and subsequent reignition followed by partially–premixed burning is observed on the "fuel–rich" side. The premixed region of the non–premixed flame has a higher reaction rate and broader reaction zone than the non–premixed flame.
- The turbulence near the flame is weakened primarily by a 25-fold increase in kinematic viscosity across the flame. The turbulence is weaker on the fuel side of the flame as a result of higher temperatures in this region.

ACKNOWLEDGEMENTS

This research was supported by the Department of Energy, Division of Basic Energy Sciences and by the Center for Turbulence Research at Stanford University/NASA–Ames. We would like to thank A. Liñán, T. Poinsot, A. Trouvé, and T. Echekki for many insightful discussions.

REFERENCES

1. J. Chen, S. Mahalingam, I. Puri, and L. Vervisch, *Proceedings of the 1992 Summer Program,* Center for Turbulence Research, NASA Ames/Stanford Univ., pp. 367-387, 1992a.
2. J. Chen, S. Mahalingam , I. Puri, and L. Vervisch, *Proceedings of the 1992 Summer Program,* Center for Turbulence Research, NASA Ames/Stanford Univ., pp. 389-402, 1992b.
3. S. Mahalingam, J. H. Chen, and L. Vervisch, *Comb. & Flame* (in press), 1994.
4. M. D. Smooke (ED.), *Reduced Kinetic Mechanisms and Asymptotic Approximation for Methane-Air Flames,* Lecture Notes in Physics 384, Springer-Verlag, New York, 1991.
5. R. J. Kee, F. M. Rupley, and J. A. Miller, *SAND-8215B,* 1987.
6. S. Lele, *J. Comput. Phys.,* vol. 103, pp. 16–42, 992.
7. T. Poinsot and S. Lele, *J. Comput. Phys,* vol. 101, No 1, 1991.
8. M. N. Bui-Pham, *Ph.D. Dissertation,* University of California, San Diego, 1992.
9. K. Seshadri and N. Peters, *Comb. & Flame,* vol. 73, pp. 23, 988.
10. I. Wichman, *Environmental Implications of Combustion Processes,* Ed. I. Puri, 1993.

DISCLAIMER